

Improved Accuracy of High-Order WENO Finite Volume Methods on Cartesian Grids*

Pawel Buchmüller[†] and Christiane Helzel[‡]

Department of Mathematics, Ruhr-University Bochum

January 29, 2014

Abstract

We propose a simple modification of standard WENO finite volume methods for Cartesian grids, which retains the full spatial order of accuracy of the one-dimensional discretization when applied to nonlinear multidimensional systems of conservation laws.

We derive formulas, which allow us to compute high-order accurate point values of the conserved quantities at grid cell interfaces. Using those point values, we can compute a high-order flux at the center of a grid cell interface. Finally, we use those point values to compute high-order accurate averaged fluxes at cell interfaces as needed by a finite volume method.

The method is described in detail for the two-dimensional Euler equations of gas dynamics. An extension to the three-dimensional case as well as to other nonlinear systems of conservation laws in divergence form is straightforward. Furthermore, similar ideas can be used to improve the accuracy of WENO type methods for hyperbolic systems which are not in divergence form.

Several test computations confirm the high-order accuracy for smooth nonlinear problems.

Keywords: Weighted essentially non-oscillatory (WENO) schemes Finite volume methods high-order methods Euler equations

1 Introduction

High-order WENO (i.e., weighted essentially non-oscillatory) methods are widely used for the approximation of hyperbolic problems, see for example the recent review of Shu [20]. The simplest way to use WENO methods on multidimensional Cartesian grids consists in applying a one-dimensional WENO scheme in each direction. This spatial discretization is typically combined with a Runge–Kutta method in time, i.e. during each stage of the Runge–Kutta method one-dimensional WENO schemes are used in a dimension–by–dimension fashion.

On uniform Cartesian grids, conservative finite difference WENO methods based on flux interpolation, as introduced by Shu and Osher [21, 22], lead to high order accurate approximations of the conserved quantities for linear as well as nonlinear conservation laws. An extension to smoothly varying mapped grids is possible, see [13]. In contrast to this, finite volume WENO methods based on a dimension–by–dimension approach retain the full order of accuracy for smooth solutions of linear multi-dimensional problems but they are only second order accurate for smooth solutions of nonlinear problems, see [20, 25].

Here we restrict our considerations to finite volume WENO methods. For hyperbolic equations in divergence form, an advantage of finite volume methods is that they approximate the integral form of a conservation law which remains valid at discontinuities, where the differential form of the

*This work was supported by the DFG through FOR1048.

[†]Pawel.Buchmueller@rub.de

[‡]Corresponding author. Christiane.Helzel@rub.de

equation is not valid in the classical sense. In general it is straight forward to extend finite volume methods to unstructured grids. With a dimension-by-dimension approach we are of course limited to Cartesian grids, but not necessarily to equidistant Cartesian grids. The standard approach to avoid the loss of accuracy of the dimension-by-dimension approach is to use a multidimensional reconstruction (with WENO limiting) and a high order quadrature formula to compute fluxes at grid cell interfaces. Such methods were used on unstructured as well as on structured grids in [2, 16, 25, 6]. However, the multidimensional reconstruction and in particular the limiting of the reconstructed polynomials is quite expensive. Furthermore, such schemes require flux computations at several points per grid cell interface (i.e., at the nodes of the quadrature formula).

A method first described in the context of ENO methods in [2] and later used for the construction of WENO methods on Cartesian grids in [23, 24, 25] is most closely related to our approach in the sense that it aims to overcome the formal loss of accuracy without using a full multi-dimensional polynomial reconstruction of the conserved quantities. Instead, those authors use one-dimensional WENO reconstruction to obtain a high-order accurate approximation of face-averaged values of the conserved quantities at all grid cell interfaces. In a second reconstruction step, these averaged values at grid cell interfaces are used to construct a one-dimensional polynomial representation of the conserved quantities along grid cell interfaces. Thus, for each grid cell interface, a one dimensional WENO reconstruction is required in the x as well as the y -direction. Finally, the method of [25] computes fluxes at grid cell interfaces by using a high-order accurate quadrature formula, thus it requires the evaluation of the numerical flux at all nodes of the quadrature formula.

Here we present a simpler modification of finite volume WENO methods, which also leads to the full spatial order of accuracy by using only one-dimensional polynomial reconstructions in a dimension-by-dimension approach. While WENO reconstruction is typically of odd order (here we consider methods of order five and seven), the corrections introduced in this paper lead to fluxes of even order (here we present the formulas for order four and six). For the temporal discretization we use explicit Runge-Kutta methods of order five or seven. An important component of our approach is the transfer of high-order averaged values of the conserved quantities to high-order point values and vice versa. Such a transformation has also been used in the recently proposed fourth order accurate finite volume method of McCorquodale and Colella [12].

In this paper we restrict our considerations to finite volume WENO methods on equidistant Cartesian grids, i.e. a case that can be handled perfectly well by finite difference WENO methods. Even on such grids, there are situations where finite volume methods are more appropriate than finite difference methods. For example, if we want to construct a high order accurate and conservative method that uses adaptive mesh refinement (AMR), see [18] for more discussions.

2 The dimension-by-dimension WENO finite volume method for hyperbolic problems in divergence form

In this section we give a brief description of Cartesian grid WENO methods and review their accuracy for linear and nonlinear multidimensional problems.

We consider two-dimensional systems of conservation laws, i.e. initial value problems of the form

$$\begin{aligned} \partial_t q + \partial_x f(q) + \partial_y g(q) &= 0 \\ q(x, y, 0) &= q_0(x, y) \end{aligned} \tag{1}$$

where $q : \mathbb{R}^2 \times \mathbb{R}^+ \rightarrow \mathbb{R}^m$ is a vector of conserved quantities, and $f, g : \mathbb{R}^m \rightarrow \mathbb{R}^m$ are vector valued flux functions.

In order to discretize (1), we use a method of lines approach. We restrict our considerations to equidistant Cartesian grids with grid cells $C_{i,j} = (x_{i-\frac{1}{2}}, x_{i+\frac{1}{2}}) \times (y_{j-\frac{1}{2}}, y_{j+\frac{1}{2}})$ and mesh width $\Delta x = x_{i+\frac{1}{2}} - x_{i-\frac{1}{2}}$ and $\Delta y = y_{j+\frac{1}{2}} - y_{j-\frac{1}{2}}$ for all i, j . A finite volume method can be written in the semi-discrete form

$$\frac{d}{dt} Q_{i,j}(t) = -\frac{1}{\Delta x} \left(F_{i+\frac{1}{2},j}(t) - F_{i-\frac{1}{2},j}(t) \right) - \frac{1}{\Delta y} \left(G_{i,j+\frac{1}{2}}(t) - G_{i,j-\frac{1}{2}}(t) \right), \tag{2}$$

where $Q_{i,j}(t)$ is an approximation of the cell average of the conserved quantities in grid cell $C_{i,j}$ and the terms $F(t), G(t)$ are flux functions at the grid cell interfaces in the x and the y -direction, respectively. For the temporal discretization we use explicit Runge-Kutta methods of appropriate

order of accuracy. The two different Runge-Kutta methods, RK5 and RK7, used for our computations are described in Appendix A.

For the spatial discretization we use in each direction a one-dimensional piecewise polynomial reconstruction of the conserved quantities. In the x -direction we construct one-dimensional polynomials $q_{i,j}^1(x)$ and in the y -direction we construct polynomials $q_{i,j}^2(y)$. These polynomials are local approximations of the conserved quantity in cell $C_{i,j}$. Furthermore, they satisfy

$$\begin{aligned} Q_{i,j} &= \frac{1}{\Delta x} \int_{x_{i-\frac{1}{2}}}^{x_{i+\frac{1}{2}}} q_{i,j}^1(x) dx \\ &= \frac{1}{\Delta y} \int_{y_{j-\frac{1}{2}}}^{y_{j+\frac{1}{2}}} q_{i,j}^2(y) dy. \end{aligned} \quad (3)$$

For each grid cell of a two-dimensional Cartesian grid, we reconstruct four edge averaged values of the conserved quantities by evaluating these polynomials at the interfaces. Those interface values of the conserved quantities are denoted by

$$\begin{aligned} Q_{i-\frac{1}{2},j}^+ &:= q_{i,j}^1(x_{i-\frac{1}{2}}), & Q_{i+\frac{1}{2},j}^- &:= q_{i,j}^1(x_{i+\frac{1}{2}}), \\ Q_{i,j-\frac{1}{2}}^+ &:= q_{i,j}^2(y_{j-\frac{1}{2}}), & Q_{i,j+\frac{1}{2}}^- &:= q_{i,j}^2(y_{j+\frac{1}{2}}). \end{aligned} \quad (4)$$

Here we use component-wise WENO reconstruction of order five and seven, known as WENO-Z method, see Appendix B. Note that at each grid cell interface we have two reconstructed edge-averaged values of the conserved quantities. Assuming that the WENO reconstruction was based on exact cell average values of the conserved quantities, then the edge averaged values satisfy (for sufficiently smooth functions q)

$$\begin{aligned} Q_{i-\frac{1}{2},j}^\pm(t) &= \frac{1}{\Delta y} \int_{y_{j-\frac{1}{2}}}^{y_{j+\frac{1}{2}}} q(x_{i-\frac{1}{2}}, y, t) dy + \mathcal{O}(\Delta x^p) \\ Q_{i,j-\frac{1}{2}}^\pm(t) &= \frac{1}{\Delta x} \int_{x_{i-\frac{1}{2}}}^{x_{i+\frac{1}{2}}} q(x, y_{j-\frac{1}{2}}, t) dx + \mathcal{O}(\Delta y^p) \end{aligned} \quad (5)$$

with $p = 5$ or $p = 7$, respectively. In general, the cell averaged values are only p -th order accurate approximations of the exact cell averaged values, i.e.

$$Q_{i,j}(t) = \frac{1}{\Delta x \Delta y} \int_{y_{j-\frac{1}{2}}}^{y_{j+\frac{1}{2}}} \int_{x_{i-\frac{1}{2}}}^{x_{i+\frac{1}{2}}} q(x, y, t) dx dy + \mathcal{O}(\Delta x^p + \Delta y^p). \quad (6)$$

We then get, for both equations of (5), on the right hand side an error of the form $\mathcal{O}(\Delta x^p + \Delta y^p)$.

The numerical fluxes $F_{i-\frac{1}{2},j}(t)$ and $G_{i,j-\frac{1}{2}}(t)$ can be obtained by using a numerical flux function such as Lax-Friedrichs, which has the form

$$F_{i-\frac{1}{2},j} = \frac{1}{2} \left[f(Q_{i-\frac{1}{2},j}^-) + f(Q_{i-\frac{1}{2},j}^+) - \alpha(Q_{i-\frac{1}{2},j}^+ - Q_{i-\frac{1}{2},j}^-) \right], \quad (7)$$

where α is an upper estimate for the largest absolute value of the eigenvalues of the flux Jacobian matrix.

Alternatively, we can compute an interface value $Q_{i-\frac{1}{2},j}^*$ of the conserved quantities, by exact or approximative solution of the Riemann problem with data $Q_{i-\frac{1}{2},j}^\pm$. The flux can then be computed using $F_{i-\frac{1}{2},j} = f(Q_{i-\frac{1}{2},j}^*)$.

Remark 1 For the computation of smooth solution of the Euler equation, the choice of the numerical flux function has only a very small effect on the quality of the numerical solutions in high-order WENO methods. Therefore, we used the Lax-Friedrichs flux function for the convergence studies shown in Section 6. For the computation of problems with shock waves or contact discontinuities, the choice of the numerical flux function has a larger impact on the quality of the numerical solution. For such problems we used the Roe Riemann solver, with an entropy fix according to Harten and Hyman, in order to compute the conserved quantity at the grid cell interfaces and evaluate the flux for this value.

In the linear case, i.e. for $f(q) = Aq$ with a constant matrix $A \in \mathbb{R}^{m \times m}$, we obtain (by using the Lax–Friedrichs flux)

$$\begin{aligned} F_{i-\frac{1}{2},j} &= \frac{1}{2} \left[A(Q_{i-\frac{1}{2},j}^- + Q_{i-\frac{1}{2},j}^+) - \alpha(Q_{i-\frac{1}{2},j}^+ - Q_{i-\frac{1}{2},j}^-) \right] \\ &= \frac{1}{2} A \frac{2}{\Delta y} \int_{y_{j-\frac{1}{2}}}^{y_{j+\frac{1}{2}}} q(x_{i-\frac{1}{2}}, y, t) dy + \mathcal{O}(\Delta x^p + \Delta y^p) \\ &= \frac{1}{\Delta y} \int_{y_{j-\frac{1}{2}}}^{y_{j+\frac{1}{2}}} Aq(x_{i-\frac{1}{2}}, y, t) dy + \mathcal{O}(\Delta x^p + \Delta y^p), \end{aligned}$$

and thus a p -th order accurate approximation of the average value of the flux across the interface. This is exactly what is needed in order to construct a p -th order accurate finite volume scheme. Interfaces in the y -direction are treated analogously.

In the nonlinear case, the dimension-by-dimension approach is in general only second order accurate. The reason for this loss of accuracy is that a flux function applied to edge averaged values of the conserved quantities does not provide an averaged flux of the same accuracy. This explains the different accuracy of multi-dimensional finite difference and finite volume WENO methods, see [20, 25]. While finite difference WENO methods retain the full order of accuracy of the one-dimensional reconstruction, finite volume WENO methods are in general only second order accurate.

The p -th order accurate edge average value $Q_{i-\frac{1}{2},j}^\pm(t)$ provides a second order accurate approximation of the point value of the conserved quantities at the midpoint of the cell edge, i.e.

$$\begin{aligned} Q_{i-\frac{1}{2},j}^\pm(t) &= \frac{1}{\Delta y} \int_{y_{j-\frac{1}{2}}}^{y_{j+\frac{1}{2}}} q(x_{i-\frac{1}{2}}, y, t) dy + \mathcal{O}(\Delta x^p) \\ &= q(x_{i-\frac{1}{2}}, y_j, t) + \mathcal{O}(\Delta y^2 + \Delta x^p). \end{aligned} \quad (8)$$

This can be interpreted as using the midpoint rule to approximate the integral on the right hand side of (8). Using the Lax-Friedrichs flux (7) and assuming that the flux function f can be expanded using Taylor series expansion, we get

$$F_{i-\frac{1}{2},j}(t) = f(q(x_{i-\frac{1}{2}}, y_j, t)) + \mathcal{O}(\Delta x^p + \Delta y^2). \quad (9)$$

Furthermore, we have

$$f(q(x_{i-\frac{1}{2}}, y_j, t)) = \frac{1}{\Delta y} \int_{y_{j-\frac{1}{2}}}^{y_{j+\frac{1}{2}}} f(q(x_{i-\frac{1}{2}}, y, t)) dy + \mathcal{O}(\Delta y^2). \quad (10)$$

From (9) and (10) we conclude that

$$F_{i-\frac{1}{2},j}(t) = \frac{1}{\Delta y} \int_{y_{j-\frac{1}{2}}}^{y_{j+\frac{1}{2}}} f(q(x_{i-\frac{1}{2}}, y, t)) dy + \mathcal{O}(\Delta x^p + \Delta y^2). \quad (11)$$

Thus the resulting WENO method is in general only second order accurate in space. We now summarize the dimension-by-dimension WENO method.

Algorithm: Dimension-by-dimension WENO method.

1. Compute averaged values of the conserved quantities at grid cell interfaces using one-dimensional WENO reconstruction, i.e. compute

$$Q_{i-\frac{1}{2},j}^\pm(t), Q_{i,j-\frac{1}{2}}^\pm(t)$$

at all grid cell interfaces.

2. Compute fluxes at grid cell interfaces using a consistent numerical flux function (such as Lax-Friedrichs), i.e.

$$F_{i-\frac{1}{2},j}(t) = \mathcal{F}(Q_{i-\frac{1}{2},j}^-, Q_{i-\frac{1}{2},j}^+), \quad G_{i,j-\frac{1}{2}}(t) = \mathcal{F}(Q_{i,j-\frac{1}{2}}^-, Q_{i,j-\frac{1}{2}}^+)$$

3. Approximate the semi-discrete system (2), using a high-order accurate Runge–Kutta method.

3 A modification of the dimension–by–dimension approach

We now describe a simple modification of the WENO method, which increases the accuracy of the dimension–by–dimension approach. With this modification, full order of accuracy can be retained for multidimensional nonlinear problems. The method is computationally less expensive than the method used in [23, 24, 25], since it is based on the one–dimensional reconstructions used in the dimension–by–dimension approach. Furthermore, our approach requires only one evaluation of the flux function per interface.

WENO reconstruction provides us with high order accurate approximations of averaged values of the conserved quantities at grid cell interfaces. For conservation laws with nonlinear flux functions, we can not directly compute high order accurate averaged values of the interface flux from these edge averaged values of the conserved quantities.

In order to compute accurate flux functions, we first compute point values of the conserved quantities at the midpoint of the grid cell interface. We then compute the numerical flux at the point value and finally compute averaged values of the flux at grid cell interfaces.

3.1 Transformation between average values and point values

We discuss the transformation between average values and point values for functions of one spatial variable. This agrees with the situation which will later be used in our method, since the second variable at grid cell interfaces will just lead to an additional index. Furthermore, we often suppress the time dependence of the functions in this subsection.

We denote with Q_i an approximation of the cell average of the function q in grid cell i , i.e. the interval $(x_{i-\frac{1}{2}}, x_{i+\frac{1}{2}})$ and by q_i an approximation of the point value $q(x_i)$ of the quantities q at the midpoint x_i of the grid cell. For sufficiently smooth functions $q : \mathbb{R} \rightarrow \mathbb{R}^m$, Taylor series expansion provides

$$\begin{aligned} Q_i &= \frac{1}{\Delta x} \int_{x_{i-\frac{1}{2}}}^{x_{i+\frac{1}{2}}} q(x) dx = \frac{1}{\Delta x} \int_{-\frac{\Delta x}{2}}^{\frac{\Delta x}{2}} q(x_i + x) dx \\ &= \frac{1}{\Delta x} \int_{-\frac{\Delta x}{2}}^{\frac{\Delta x}{2}} \left(q(x_i) + xq'(x_i) + \frac{x^2}{2}q''(x_i) + \frac{x^3}{6}q'''(x_i) + \frac{x^4}{24}q^{(4)}(x_i) + \dots \right) dx \end{aligned}$$

and thus the transformation

$$q_i = Q_i - \frac{\Delta x^2}{24}q''(x_i) - \frac{\Delta x^4}{1920}q^{(4)}(x_i) + \dots \quad (12)$$

between point values and cell average values.

Thus we need expressions for the approximation of second and fourth derivatives. In order to transform from point values to cell average values, we can approximate these derivatives using standard finite difference formulas. If we transform from cell average values to point values, we use cell average values of the conserved quantities in order to approximate the second and fourth derivative at the midpoint of the interval.

3.1.1 Approximation of derivatives from point values

The second derivative $q''(x_i)$ can be approximated using point values of the quantity q via the well known second order accurate FD formula

$$q''(x_i) = \frac{1}{\Delta x^2} (q_{i-1} - 2q_i + q_{i+1}) + \mathcal{O}(\Delta x^2). \quad (13)$$

A fourth order accurate representation of $q''(x_i)$ can be obtained using the formula

$$q''(x_i) = \frac{1}{12\Delta x^2} (-q_{i-2} + 16q_{i-1} - 30q_i + 16q_{i+1} - q_{i+2}) + \mathcal{O}(\Delta x^4). \quad (14)$$

A second order accurate representation of $q^{(4)}(x_i)$ can be computed from point values using the finite difference formula

$$q^{(4)}(x_i) = \frac{1}{\Delta x^4} (q_{i-2} - 4q_{i-1} + 6q_i - 4q_{i+1} + q_{i+2}) + \mathcal{O}(\Delta x^2). \quad (15)$$

All of these formulas can be verified using Taylor series expansion.

3.1.2 Approximation of derivatives from cell average values

Second order accurate approximations of $q''(x_i)$ and $q^{(4)}(x_i)$ can be obtained using formulas analogously to (13) and (15) with the point values q_i replaced by average values Q_i .

A fourth order accurate approximation of $q''(x_i)$ can be computed from cell averaged values via the formula

$$q''(x_i) = \frac{1}{8\Delta x^2} (-Q_{i-2} + 12Q_{i-1} - 22Q_i + 12Q_{i+1} - Q_{i+2}) + \mathcal{O}(\Delta x^4). \quad (16)$$

This formula can also be verified by Taylor series expansion, after using (12) to express the cell average values by point values.

Note that the equations (13)-(16) are only valid for uniform Cartesian grids. Similar formulas can be derived for nonuniform Cartesian grids.

3.2 Modification of the dimension-by-dimension WENO method

The considerations of the previous section suggest the following modification of the dimension-by-dimension finite volume WENO method.

Algorithm: Modified dimension-by-dimension WENO method

1. Compute averaged values of the conserved quantities at grid cell interfaces using one-dimensional WENO reconstruction, i.e. compute

$$Q_{i-\frac{1}{2},j}^{\pm}(t), Q_{i,j-\frac{1}{2}}^{\pm}(t)$$

at all grid cell interfaces.

2. Compute point values of the conserved quantities at the midpoints of grid cell interfaces, i.e. compute

$$q_{i-\frac{1}{2},j}^{\pm}(t), q_{i,j-\frac{1}{2}}^{\pm}(t)$$

using the transformation (12).

3. Compute fluxes at midpoints of the grid cell interfaces using a consistent numerical flux function, i.e.

$$f_{i-\frac{1}{2},j}(t) = \mathcal{F}(q_{i-\frac{1}{2},j}^-, q_{i-\frac{1}{2},j}^+), \quad g_{i,j-\frac{1}{2}}(t) = \mathcal{F}(q_{i,j-\frac{1}{2}}^-, q_{i,j-\frac{1}{2}}^+)$$

4. Compute averaged values of the flux, denoted by $F_{i-\frac{1}{2},j}(t)$ and $G_{i,j-\frac{1}{2}}(t)$, at grid cell interfaces using the transformation (12).

5. Approximate the semi-discrete system (2), using a high-order accurate Runge-Kutta method.

Different versions of this method can now be considered depending 1.) on the number of terms on the right hand side of (12), which are used to transform between cell average values and point values and 2.) on the choice of the formula used to discretize the derivatives in (12).

We consider the following variations of the method. In the different methods, the cell averaged values of the conserved quantities $Q_{i-\frac{1}{2},j}^{\pm}$ and $Q_{i,j-\frac{1}{2}}^{\pm}$ are computed using either fifth or seventh order WENO reconstruction.

- **method 1:** The standard dimension-by-dimension approach.
- **method 2:** Point values of the conserved quantities at midpoints of grid cell interfaces are computed using

$$\begin{aligned} q_{i-\frac{1}{2},j}^{\pm} &= Q_{i-\frac{1}{2},j}^{\pm} - \frac{1}{24} \left(Q_{i-\frac{1}{2},j-1}^{\pm} - 2Q_{i-\frac{1}{2},j}^{\pm} + Q_{i-\frac{1}{2},j+1}^{\pm} \right) \\ q_{i,j-\frac{1}{2}}^{\pm} &= Q_{i,j-\frac{1}{2}}^{\pm} - \frac{1}{24} \left(Q_{i-1,j-\frac{1}{2}}^{\pm} - 2Q_{i,j-\frac{1}{2}}^{\pm} + Q_{i+1,j-\frac{1}{2}}^{\pm} \right) \end{aligned} \quad (17)$$

The numerical fluxes used in (2) are computed from point values of the flux using the relations

$$\begin{aligned} F_{i-\frac{1}{2},j} &= f_{i-\frac{1}{2},j} + \frac{1}{24} \left(f_{i-\frac{1}{2},j-1} - 2f_{i-\frac{1}{2},j} + f_{i-\frac{1}{2},j+1} \right) \\ G_{i,j-\frac{1}{2}} &= g_{i,j-\frac{1}{2}} + \frac{1}{24} \left(g_{i-1,j-\frac{1}{2}} - 2g_{i,j-\frac{1}{2}} + g_{i+1,j-\frac{1}{2}} \right) \end{aligned} \quad (18)$$

- **method 3:** Point values of the conserved quantities at grid cell interfaces are computed using

$$\begin{aligned}
q_{i-\frac{1}{2},j}^{\pm} &= Q_{i-\frac{1}{2},j}^{\pm} \\
&- \frac{1}{24} \left(-\frac{1}{8} Q_{i-\frac{1}{2},j-2}^{\pm} + \frac{3}{2} Q_{i-\frac{1}{2},j-1}^{\pm} - \frac{11}{4} Q_{i-\frac{1}{2},j}^{\pm} + \frac{3}{2} Q_{i-\frac{1}{2},j+1}^{\pm} - \frac{1}{8} Q_{i-\frac{1}{2},j+2}^{\pm} \right) \\
&- \frac{1}{1920} \left(Q_{i-\frac{1}{2},j-2}^{\pm} - 4Q_{i-\frac{1}{2},j-1}^{\pm} + 6Q_{i-\frac{1}{2},j}^{\pm} - 4Q_{i-\frac{1}{2},j+1}^{\pm} + Q_{i-\frac{1}{2},j+2}^{\pm} \right) \\
&= Q_{i-\frac{1}{2},j}^{\pm} - \left(-\frac{3}{640} Q_{i-\frac{1}{2},j-2}^{\pm} + \frac{29}{480} Q_{i-\frac{1}{2},j-1}^{\pm} - \frac{107}{960} Q_{i-\frac{1}{2},j}^{\pm} \right. \\
&\quad \left. + \frac{29}{480} Q_{i-\frac{1}{2},j+1}^{\pm} - \frac{3}{640} Q_{i-\frac{1}{2},j+2}^{\pm} \right)
\end{aligned} \tag{19}$$

and by an analogous formula for $q_{i,j-\frac{1}{2}}^{\pm}$.

The interface fluxes are computed from point values of the fluxes using

$$\begin{aligned}
F_{i-\frac{1}{2},j} &= f_{i-\frac{1}{2},j} \\
&+ \frac{1}{24} \left(-\frac{1}{12} f_{i-\frac{1}{2},j-2} + \frac{4}{3} f_{i-\frac{1}{2},j-1} - \frac{5}{2} f_{i-\frac{1}{2},j} + \frac{4}{3} f_{i-\frac{1}{2},j+1} - \frac{1}{12} f_{i-\frac{1}{2},j+2} \right) \\
&+ \frac{1}{1920} \left(f_{i-\frac{1}{2},j-2} - 4f_{i-\frac{1}{2},j-1} + 6f_{i-\frac{1}{2},j} - 4f_{i-\frac{1}{2},j+1} + f_{i-\frac{1}{2},j+2} \right)
\end{aligned} \tag{20}$$

and an analogous formula for $G_{i,j-\frac{1}{2}}$.

In Figures 1 and 2 we show the stencil used in one time stage of our method using 5th order WENO reconstruction together with the modification implemented in method 2. In the left part of Figure 1, we show the stencil which is used in order to compute edge averaged values of the conserved quantities marked as two dashed lines. In a standard dimension-by-dimension approach, those edge averaged values are used to compute the interface flux. In our modified method, we compute point values of the conserved quantities using equation (17). For this computation we need neighboring edge averaged values, which enlarges the stencil as indicated in the right part of Figure 1. The point values of the conserved quantity (indicated by black dots) are used to compute point values of the flux (indicated by the open ellipse.)

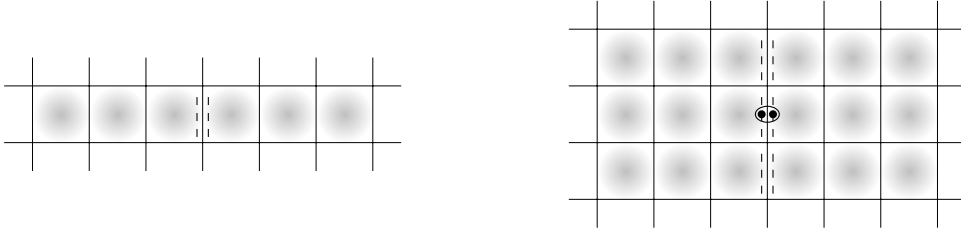


Figure 1: The left plot shows the stencil for the computation of $Q_{i-\frac{1}{2},j}^{\pm}$. These averaged interface values are indicated by the two dashed lines. The right plot shows the stencil for the computation of the point values $q_{i-\frac{1}{2},j}^{\pm}$, indicated as black dots in the figure. Those point values are used to compute point values of the flux, denoted by $f_{i-\frac{1}{2},j}$. The point value of the flux is marked as an open ellipse.

In the left plot of Figure 2, we show the stencil needed to compute edge averaged values of the flux according to equation (18). This transformation requires neighboring point values of fluxes, which further enlarges the stencil. In the right plot of Figure 2 we show the full stencil of cells that are used to update one cell. The dark shaded grid cells are those used in the classical dimension-by-dimension WENO method. Note that after computing all fluxes (of the modified method) for one cell, most of the work for the neighboring cells is already done. Therefore, the larger stencil only leads to a relatively small increase of the computational costs, as shown below in Table 6.

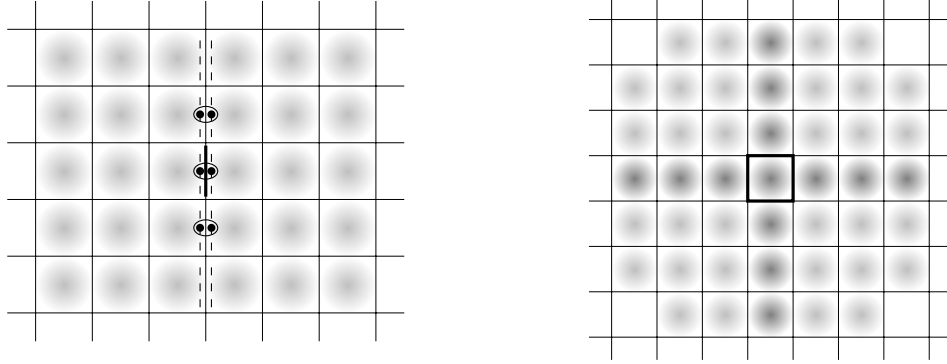


Figure 2: The left plot shows the stencil, which is used in order to compute the cell averaged value of the flux at the interface, i.e. $F_{i-\frac{1}{2},j}$. This flux is marked as a dark solid line. The right plot shows the complete stencil used to update the grid cell in the center. The dark shaded cells are used in a classical dimension-by-dimension approach, i.e. by method 1.

Remark 2 We can replace the flux computation in (18) by a formula of the form

$$F_{i-\frac{1}{2},j} = f_{i-\frac{1}{2},j} + \frac{1}{24} \left(\bar{f}_{i-\frac{1}{2},j-1} - 2\bar{f}_{i-\frac{1}{2},j} + \bar{f}_{i-\frac{1}{2},j+1} \right), \quad (21)$$

and analogously for $G_{i,j-\frac{1}{2}}$, where $\bar{f}_{i-\frac{1}{2},k} = \mathcal{F}(Q_{i-\frac{1}{2},k}^-, Q_{i-\frac{1}{2},k}^+)$, $k = j-1, j, j+1$, is a flux computed using the averaged values of the conserved quantities. The resulting finite volume method has a more local stencil. (For WENO5 the 16 most outer light shaded cells in the right plot of Figure 2 would not be used.) However, this approach requires the computation of two fluxes per interface. We have also tested such versions of the method and obtained good results. These computations will not be presented here.

Finally, in Table 1, we summarize the expected convergence rates of the different methods for

method	WENO5+RK5		WENO7+RK7	
	linear	nonlinear	linear	nonlinear
method 1	5	2	7	2
method 2	4	4	4	4
method 3	5	5	6	6

Table 1: Predicted convergence rate for the approximation of smooth problems with the different numerical methods.

the approximation of linear and nonlinear problems.

4 Nonlinear systems in quasilinear form

In a recent paper, Ketcheson et al. [10] used WENO reconstruction to develop high-order wave propagation methods for hyperbolic equations in the quasilinear form

$$q_t + A(q)q_x + B(q)q_y = 0. \quad (22)$$

Their numerical method can be written in the semi-discrete form

$$\begin{aligned} \frac{d}{dt} Q_{i,j}(t) = & -\frac{1}{\Delta x} \left(\mathcal{A}^- \Delta Q_{i+\frac{1}{2},j} + \mathcal{A}^+ \Delta Q_{i-\frac{1}{2},j} + \mathcal{A} \Delta Q_{i,j} \right) \\ & -\frac{1}{\Delta y} \left(\mathcal{B}^- \Delta Q_{i,j+\frac{1}{2}} + \mathcal{B}^+ \Delta Q_{i,j-\frac{1}{2}} + \mathcal{B} \Delta Q_{i,j} \right), \end{aligned} \quad (23)$$

where $\mathcal{A}^\pm \Delta Q$ and $\mathcal{B}^\pm \Delta Q$ are fluctuations which are computed using an eigenvector decomposition of the jump of the piecewise polynomial reconstructed quantity q at each grid cell interface as

explained in [10, 11]. The two–dimensional version of the method in [10] is based on a dimension–by–dimension WENO reconstruction of q . It is second order accurate for smooth solutions of nonlinear hyperbolic systems in analogy to the dimension–by–dimension approach for nonlinear hyperbolic systems in divergence form.

The approach suggested in this paper to obtain high order of accuracy can be extended to hyperbolic systems of the form (22). The computation of the terms $\mathcal{A}^\pm \Delta Q$ and $\mathcal{B}^\pm \Delta Q$ can be done in analogy to the flux computation, i.e. by first computing high order point values of q at the interfaces, by using these values to compute high–order accurate point values of the fluctuations, and finally by computing grid cell interface averaged values of the fluctuations from the point values of the fluctuations.

The discretization of $\mathcal{A}\Delta Q_{i,j}$ and $\mathcal{B}\Delta Q_{i,j}$ requires some additional transformations. Consider the discretization of

$$\mathcal{A}\Delta Q_{i,j} \approx \frac{1}{\Delta y} \int_{y_{j-\frac{1}{2}}}^{y_{j+\frac{1}{2}}} \int_{x_{i-\frac{1}{2}}}^{x_{i+\frac{1}{2}}} A(q(x,y,t))q_x(x,y,t)dx dy. \quad (24)$$

Let $x_{i-\frac{1}{2}} \leq x_1 < \dots < x_\ell \leq x_{i+\frac{1}{2}}$ and c_1, \dots, c_ℓ denote the nodes and weights of a quadrature formula, which can be written in the general form

$$Q[f] = \sum_{k=1}^{\ell} c_k f(x_k) \approx \int_{x_{i-\frac{1}{2}}}^{x_{i+\frac{1}{2}}} f(x)dx. \quad (25)$$

Furthermore, let $q_{i,j}^1(x)$, $x_{i-\frac{1}{2}} < x < x_{i+\frac{1}{2}}$ denote the p -th order accurate WENO reconstruction in the x -direction of the quantity q in cell (i,j) , compare with Section 2. The evaluation of $q_{i,j}^1$ at a quadrature node provides us with a point value of q in the x -direction and an averaged value of q in the y -direction, i.e.

$$q_{i,j}^1(x_k) = \frac{1}{\Delta y} \int_{y_{j-\frac{1}{2}}}^{y_{j+\frac{1}{2}}} q(x_k, y)dy + \mathcal{O}(\Delta x^p + \Delta y^p) \quad k = 1, \dots, \ell. \quad (26)$$

Furthermore, differentiating the polynomial $q_{i,j}^1$ provides us with an approximation of the averaged derivative, i.e.

$$(q_{i,j}^1)_x(x_k) = \frac{1}{\Delta y} \int_{y_{j-\frac{1}{2}}}^{y_{j+\frac{1}{2}}} q_x(x_k, y)dy + \mathcal{O}(\Delta x^{p-1} + \Delta y^p), \quad k = 1, \dots, \ell. \quad (27)$$

Using the transformation from averaged values to point values, i.e. (12), we compute approximations of the point values $q(x_k, y_j)$ and $q_x(x_k, y_j)$ for $k = 1, \dots, \ell$ and $y_j = (y_{j-\frac{1}{2}} + y_{j+\frac{1}{2}})/2$. These point values are computed using neighboring averaged values, i.e. $q_{i,j-2}^1(x_k)$, $q_{i,j-1}^1(x_k)$, $q_{i,j+1}^1(x_k)$ and $q_{i,j+2}^1(x_k)$ for $k = 1, \dots, \ell$ and analogously for the derivatives. Now we can evaluate the point values $A(q_{i,j}^1(x_k, y_j, t))q_x^1(x_k, y_j, t)$ for $k = 1, \dots, \ell$. Using again the transformation (12), we compute averaged values of these quantities in the y -direction and denote them by

$$\overline{A(q_{i,j}^1(x_k, t))q_x^1(x_k)} \approx \frac{1}{\Delta y} \int_{y_{j-\frac{1}{2}}}^{y_{j+\frac{1}{2}}} A(q(x_k, y))q_x(x_k, y)dy \quad k = 1, \dots, \ell. \quad (28)$$

These values are finally used in a one–dimensional quadrature formula of the form (25), giving an approximation of the two–dimensional integral in (24):

$$\sum_{k=1}^{\ell} c_k \overline{A(q_{i,j}^1(x_k, t))q_x^1(x_k)} = \mathcal{A}\Delta Q_{i,j}. \quad (29)$$

Analogously we can compute the term

$$\mathcal{B}\Delta Q_{i,j} \approx \frac{1}{\Delta x} \int_{y_{j-\frac{1}{2}}}^{y_{j+\frac{1}{2}}} \int_{x_{i-\frac{1}{2}}}^{x_{i+\frac{1}{2}}} B(q(x,y,t))q_y(x,y,t)dx dy. \quad (30)$$

5 Extension to higher dimensions

We now present the basic formula which is needed for an extension of the modified WENO method to higher dimensions. Let us first introduce some additional notation. For $\mathbf{x} \in \mathbb{R}^d$, $\mathbf{n} \in \mathbb{N}^d$, let $\mathbf{x}^{\mathbf{n}} = x_1^{n_1} \cdots x_d^{n_d}$, $|\mathbf{n}| = n_1 + \cdots + n_d$, $\mathbf{n}! = n_1! \cdots n_d!$ and $\mathbf{n} + \mathbf{1}! = (n_1 + 1)! \cdots (n_d + 1)!$. Furthermore we restrict our considerations to equidistant Cartesian grids and set $h = \Delta x_1 = \dots = \Delta x_d$. For $\mathbf{x}_i, \boldsymbol{\xi} \in \mathbb{R}^d$ with $|\xi_j| \leq h$, $j = 1, \dots, d$, the multidimensional Taylor series expansion yields

$$\begin{aligned} q(\mathbf{x}_i + \boldsymbol{\xi}) &= \sum_{\substack{0 \leq n_1, \dots, n_d, \\ n_1 + \dots + n_d \leq p}} \frac{\xi_1^{n_1} \cdots \xi_d^{n_d}}{n_1! \cdots n_d!} \frac{\partial^{n_1 + \dots + n_d}}{\partial x_1^{n_1} \cdots \partial x_d^{n_d}} q(\mathbf{x}_i) + \mathcal{O}(h^{p+1}) \\ &= \sum_{0 \leq |\mathbf{n}| \leq p} \frac{\boldsymbol{\xi}^{\mathbf{n}}}{\mathbf{n}!} \frac{\partial^{|\mathbf{n}|}}{\partial \mathbf{x}^{\mathbf{n}}} q(\mathbf{x}_i) + \mathcal{O}(h^{p+1}). \end{aligned} \quad (31)$$

For $\xi \in \mathbb{R}$, $n \in \mathbb{N}$ we get

$$\int_{-\frac{h}{2}}^{\frac{h}{2}} \xi^n d\xi = \frac{1}{n+1} \xi^{n+1} \Big|_{-\frac{h}{2}}^{\frac{h}{2}} = \begin{cases} 0 & \text{if } n \text{ is odd,} \\ \frac{h^{n+1}}{2^{n(n+1)}} & \text{if } n \text{ is even.} \end{cases} \quad (32)$$

For an even number p this leads to

$$\begin{aligned} Q_i &= \frac{1}{h^d} \int_{x_{i_1} - \frac{h}{2}}^{x_{i_1} + \frac{h}{2}} \cdots \int_{x_{i_d} - \frac{h}{2}}^{x_{i_d} + \frac{h}{2}} q(x_1, \dots, x_d) dx_d \dots dx_1 \\ &= \frac{1}{h^d} \int_{-\frac{h}{2}}^{\frac{h}{2}} \cdots \int_{-\frac{h}{2}}^{\frac{h}{2}} q(x_{i_1} + \xi_1, \dots, x_{i_d} + \xi_d) d\xi_d \dots d\xi_1 \\ &= \frac{1}{h^d} \sum_{0 \leq |\mathbf{n}| \leq p} \frac{\partial^{|\mathbf{n}|}}{\partial \mathbf{x}^{\mathbf{n}}} q(\mathbf{x}_i) \int_{-\frac{h}{2}}^{\frac{h}{2}} \cdots \int_{-\frac{h}{2}}^{\frac{h}{2}} \frac{\xi_1^{n_1} \cdots \xi_d^{n_d}}{\mathbf{n}!} d\xi_d \dots d\xi_1 + \mathcal{O}(h^{p+1}) \\ &= \frac{1}{h^d} \sum_{\substack{0 \leq |\mathbf{n}| \leq p, \\ n_j = 2k_j}} \frac{h^{|\mathbf{n}|+d}}{2^{|\mathbf{n}|} (\mathbf{n} + \mathbf{1})!} \frac{\partial^{|\mathbf{n}|}}{\partial \mathbf{x}^{\mathbf{n}}} q(\mathbf{x}_i) + \mathcal{O}(h^{p+2}) \\ &= q(\mathbf{x}_i) + \sum_{\substack{0 < |\mathbf{n}| \leq p, \\ n_j = 2k_j}} \frac{h^{|\mathbf{n}|}}{2^{|\mathbf{n}|} (\mathbf{n} + \mathbf{1})!} \frac{\partial^{|\mathbf{n}|}}{\partial \mathbf{x}^{\mathbf{n}}} q(\mathbf{x}_i) + \mathcal{O}(h^{p+2}). \end{aligned} \quad (33)$$

By approximating the corresponding derivatives, we can now obtain transformation formulas for any dimension and order. For $p = 2$ we retain method 2 and for $p = 4$ we retain method 3. But notice, while method 2 is a simple sum of second derivatives, higher order transformations contain also cross terms when applied in more than one dimensions. Note that at grid cell interfaces of a two-dimensional Cartesian mesh, we need to apply the one-dimensional transformation formulas ($d = 1$) and at grid cell interfaces of a three-dimensional cell we apply the two-dimensional formulas ($d = 2$).

6 Numerical results for the Euler equations of gas dynamics

In this section we present different simulations and convergence studies. We use the two-dimensional Euler equations of gas dynamics as our model problem, i.e. we consider approximations of

$$\partial_t \begin{pmatrix} \rho \\ \rho u \\ \rho v \\ E \end{pmatrix} + \partial_x \begin{pmatrix} \rho u \\ \rho u^2 + p \\ \rho uv \\ u(E + p) \end{pmatrix} + \partial_y \begin{pmatrix} \rho v \\ \rho uv \\ \rho v^2 + p \\ v(E + p) \end{pmatrix} = 0, \quad (34)$$

with the ideal gas equation of state

$$E = \frac{p}{\gamma - 1} + \frac{1}{2} \rho (u^2 + v^2). \quad (35)$$

The initial values will be specified below for each test problem. We always set $\gamma = 1.4$.

In the following subsections, we will present different tables with convergence studies. There, the $\|\cdot\|_1$ -norm of the error in density is shown for different grids. If an exact solution is available, we use those as reference solution. Otherwise, the reference solution is a numerical solution computed on a highly refined mesh. We compute the experimental order of convergence using the formula

$$EOC = \frac{\log(\|\rho_m - \rho_{ref}\|/\|\rho_{2m} - \rho_{ref}\|)}{\log 2}, \quad (36)$$

where the index m indicates the number of grid points in the x and the y direction. Note that for the other conserved variables we always obtained comparable results which are not shown here. In all computations we used time steps corresponding to $CFL \approx 0.9$.

6.1 Smooth test problems and convergence studies

6.1.1 Linear problem

Example 1 We consider periodic solutions of (34) on the domain $[0, 1] \times [0, 1]$. The initial values are given by

$$\begin{aligned} \rho(x, y, 0) &= 1 + 0.5 \sin(2\pi x) \cos(2\pi y) \\ p(x, y, 0) &= 1 \\ u(x, y, 0) &= v(x, y, 0) = 1. \end{aligned} \quad (37)$$

In this case, velocity and pressure remain constant for all times and the initial density profile is advected by the velocity field. Thus we are approximating a problem in the linear regime.

In Table 2 we show results of a numerical convergence study. Here we compute the $\|\cdot\|_1$ -norm of the error in density by comparing the solution obtained on different grids with the exact solution. In Table 2 we show results with fifth order WENO-Z reconstruction, using $\epsilon = \Delta x^4$ and $p = 2$, compare with Appendix B. In all of these computations, we used RK5 as time stepping scheme, see Appendix A.

As expected in the linear case, the simple dimension-by-dimension approach, implemented in method 1, converges with fifth order. The full order of convergence of the WENO-Z reconstruction is also retained by method 3. By using method 2, we observe a loss of accuracy and, as expected, a convergence rate of four. In Table 3 we show the results where the seventh order WENO-Z was

grid	method 1		method 2		method 3	
	$\ \rho - \rho_{exact}\ _1$	EOC	$\ \rho - \rho_{exact}\ _1$	EOC	$\ \rho - \rho_{exact}\ _1$	EOC
64^2	4.61953d-7		5.65033d-7		4.61965d-7	
128^2	1.44675d-8	5.00	2.49135d-8	4.50	1.44677d-8	5.00
256^2	4.52368d-10	5.00	1.34356d-9	4.21	4.52369d-10	5.00
512^2	1.41384d-11	5.00	8.01169d-11	4.07	1.41384d-11	5.00

Table 2: Convergence study for Example 1 with 5th order WENO-Z reconstruction and RK5. For these computations we used time steps with $CFL \approx 0.9$ and the Lax-Friedrichs flux.

combined with RK7, see Appendix B and A. Again we observe that the order of convergence is

grid	method 1		method 2		method 3	
	$\ \rho - \rho_{exact}\ _1$	EOC	$\ \rho - \rho_{exact}\ _1$	EOC	$\ \rho - \rho_{exact}\ _1$	EOC
64^2	9.52785d-10		3.21588d-7		1.11271d-9	
128^2	7.46432d-12	7.00	2.01439d-08	4.00	1.16519d-11	6.58
256^2	5.84576d-14	7.00	1.25974d-09	4.00	1.51789d-13	6.26
512^2	4.56021d-16	7.00	7.87454d-11	4.00	2.22517d-15	6.09

Table 3: Convergence study for Example 1 with 7th order WENO-Z reconstruction and RK7. For these computations we used time steps with $CFL \approx 0.9$ and the Lax-Friedrichs flux.

as expected for each of the methods. Note that for the combinations *WENO-Z5+RK5+method 2* and *WENO-Z7+RK7+method 3* we observe, at least on coarser grids, an experimental order of convergence which is above the theoretically expected order of convergence.

6.1.2 Nonlinear problems

Example 2 Now we consider the two-dimensional vortex evolution problem (see e.g. [9]) on the periodic domain $[-7, 7] \times [-7, 7]$. The initial data consist of a mean flow $\rho = u = v = p = 1$, which is perturbed by adding

$$\begin{pmatrix} \delta\rho \\ \delta u \\ \delta v \\ \delta p \end{pmatrix} = \begin{pmatrix} (1 + \delta T)^{1/(\gamma-1)} - 1 \\ -y \frac{\sigma}{2\pi} e^{0.5(1-r)} \\ x \frac{\sigma}{2\pi} e^{0.5(1-r)} \\ (1 + \delta T)^{\gamma/(\gamma-1)} - 1 \end{pmatrix}. \quad (38)$$

Here δT , the perturbation in the temperature, is given by

$$\delta T = -\frac{(\gamma-1)\sigma^2}{8\gamma\pi^2} e^{1-r^2}, \quad (39)$$

with $r^2 = x^2 + y^2$ and the vortex strength $\sigma = 5$.

In the Tables 4 and 5, we show the error and the experimental convergence rates for the approximation of density using the three different methods. Here the exact solution, which at time $t = 14$ agrees with the initial values, was used as reference solution.

In Table 4, we use the fifth order accurate WENO-Z reconstruction together with RK5, and in Table 5 we use the seventh order accurate WENO-Z reconstruction with RK7. With the dimension-by-dimension approach implemented in method 1, we obtain similar results for both reconstructions. By refining the grid, the experimental order of convergence (EOC) drops to second order, as expected for nonlinear problems. Method 2 and method 3 give almost identical results on coarser grids for the fifth order WENO-Z reconstruction. In both cases we obtain a convergence rate of about five. Only on very fine grids the lower order of method 2 became visible. By using seventh order WENO-Z reconstruction, the drop in the convergence rate of method 2 is much more obvious and can already be seen on coarser grids. As already seen in Example 1, the combinations *WENO-Z5+RK5+method 2* and *WENO-Z7+RK7+method 3* provide even better results than expected.

grid	method 1		method 2		method 3	
	$\ \rho - \rho_{exact}\ _1$	EOC	$\ \rho - \rho_{exact}\ _1$	EOC	$\ \rho - \rho_{exact}\ _1$	EOC
64^2	2.07461d-4		1.55933d-4		1.55288d-4	
128^2	2.95314d-5	2.81	8.17206d-6	4.25	8.15400d-6	4.25
256^2	7.03771d-6	2.07	2.40376d-7	5.09	2.36830d-7	5.11
512^2	1.75592d-6	2.00	7.71743d-9	4.96	7.40743d-9	5.00
1024^2	4.39556d-7	2.00	2.57207d-10	4.91	2.30667d-10	5.01
2048^2	1.09902d-7	2.00	9.41754d-12	4.77	7.20526d-12	5.00
4096^2	2.74756d-8	2.00	4.00267d-13	4.56	2.27363d-13	4.99

Table 4: Convergence study for Example 2 with fifth order accurate WENO-Z reconstruction and fifth order accurate Runge-Kutta method.

grid	method 1		method 2		method 3	
	$\ \rho - \rho_{exact}\ _1$	EOC	$\ \rho - \rho_{exact}\ _1$	EOC	$\ \rho - \rho_{exact}\ _1$	EOC
64^2	1.18318d-4		3.18576d-5		3.09485d-5	
128^2	2.80558d-5	2.08	6.08063d-7	5.71	4.85418d-7	5.99
256^2	7.01366d-6	2.00	1.96245d-8	4.95	4.34579d-9	6.80
512^2	1.75733d-6	2.00	1.20938d-9	4.02	3.46585d-11	6.97
1024^2	4.39593d-8	2.00	7.57974d-11	4.00	2.77524d-13	6.96
2048^2	1.10050d-8	2.00	4.73921d-12	4.00	2.40689d-15	6.85

Table 5: Convergence study for Example 2 with seventh order accurate WENO-Z reconstruction and seventh order accurate Runge-Kutta method.

In Table 6 we show the result of a performance-test. In order to keep the test as fair as possible we ran all performance-tests on the same machine and always exclusively. The code has been parallelized using OpenMP and each test was performed with two threads. We see that in our

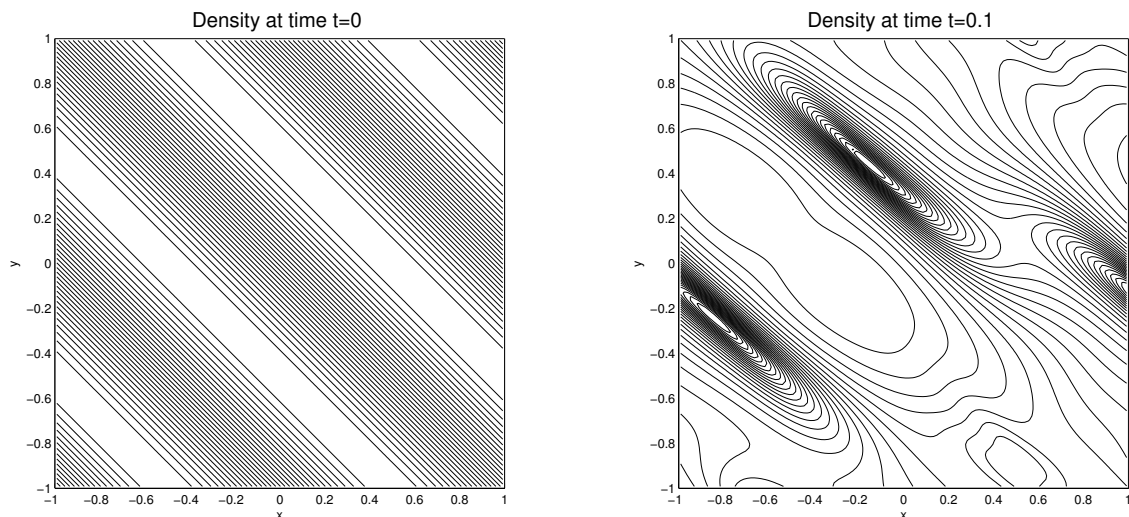


Figure 3: Contour plots for initial data and numerical solution at time $t = 0.1$ for Example 3 using 128×128 grid cells.

implementation the additional computations, needed by method 2 and method 3, increase the computational costs on average by 10%–16%. Furthermore, we observe that the relative influence is smaller for the more expensive seventh order WENO-Z reconstruction. This makes sense, since the additional computations required by our modified WENO methods are independent of the chosen reconstruction.

grid	WENO-Z5 + RK5			WENO-Z7 + RK7		
	method 1	method 2	method 3	method 1	method 2	method 3
64^2	1.00	1.09	1.12	1.00	1.07	1.09
128^2	1.00	1.15	1.18	1.00	1.10	1.12
256^2	1.00	1.15	1.17	1.00	1.10	1.12
512^2	1.00	1.15	1.17	1.00	1.10	1.12
\emptyset	1.00	1.14	1.16	1.00	1.10	1.11

Table 6: Performance-test on a Intel Core 2 Duo CPU E6850 with 3.00GHz and 2GB RAM for Example 2. Run time normalized with respect to method 1 on each grid. Compare with a performance test of the method studied by Zhang, Zhang, Shu in [25].

Example 3 Now we solve the Euler equations with initial values of the form

$$\begin{aligned}
 \rho(x, y, 0) &= 1 + \frac{1}{2} \sin(\pi(x + y)) \\
 u(x, y, 0) &= \cos(\pi(x + 2y)) \\
 v(x, y, 0) &= 1 - \frac{1}{2} \sin(\pi(2x + y)) \\
 p(x, y, 0) &= 1 + \frac{1}{2} \sin(\pi(x - y))
 \end{aligned} \tag{40}$$

in the domain $[-1, 1] \times [-1, 1]$ with periodicity condition. The solution will be computed at time $t = 0.1$ and compared to the solution at different grids with a reference solution computed using method 3 with seventh order reconstruction and RK7 on a grid with 4096×4096 grid cells.

Figure 3 shows the solution structure for Example 3. In Table 7 we present a convergence study for Example 3 using the three different methods with WENO-Z5 and RK5. We observe the same behavior as in Example 2. With the standard dimension-by-dimension approach, the method converges with second order. We clearly see the improved accuracy of method 2 and method 3 compared to the standard approach used in method 1. But only on the very finest grid we see a considerable difference between method 2 and method 3.

grid	method 1		method 2		method 3	
	$\ \rho - \rho_{ref}\ _1$	EOC	$\ \rho - \rho_{ref}\ _1$	EOC	$\ \rho - \rho_{ref}\ _1$	EOC
64^2	2.00097d-3		1.32954d-3		1.36177d-3	
128^2	4.88291d-4	2.03	7.77433d-5	4.10	8.06215d-5	4.08
256^2	1.25512d-4	1.96	2.57926d-6	4.91	2.76102d-6	4.87
512^2	3.15995d-5	1.99	7.48302d-8	5.11	8.43834d-8	5.03
1024^2	7.90940d-6	2.00	2.25639d-9	5.05	2.55045d-9	5.05
2048^2	1.97774d-6	2.00	9.55098d-11	4.56	7.72001d-11	5.05

Table 7: Convergence study for Example 3 with fifth order accurate WENO-Z reconstruction and fifth order accurate Runge-Kutta method. The reference solution was computed using method 3 with seventh order WENO-Z reconstruction and RK7 on a grid with 4096×4096 grid cells.

In Table 8 we show the results of a numerical convergence study of Example 3 using the three different methods with WENO-Z7 and RK7. For the dimension-by-dimension approach, the higher order spatial reconstruction did not lead to any increase in accuracy, compared to method 1 with WENO-Z5. The same holds for method 2 on the finest grids. For method 2 on coarse grids and for method 3 we do observe the gain in accuracy due to the higher order reconstruction. With this higher order spatial reconstruction we also observe the expected fourth order convergence rate of method 2. Furthermore, we observe that the use of method 3 leads to a smaller error if compared to method 2.

grid	method 1		method 2		method 3	
	$\ \rho - \rho_{ref}\ _1$	EOC	$\ \rho - \rho_{ref}\ _1$	EOC	$\ \rho - \rho_{ref}\ _1$	EOC
64^2	1.84119d-3		5.01165d-4		5.15434d-4	
128^2	5.01723d-4	1.88	1.14852d-5	5.45	1.01807d-5	5.66
256^2	1.26335d-4	1.99	4.44425d-7	4.69	1.06754d-7	6.58
512^2	3.16297d-5	2.00	2.85272d-8	3.96	8.64458d-10	6.95
1024^2	7.91038d-6	2.00	1.79754d-9	3.99	6.60027d-12	7.03
2048^2	1.97777d-6	2.00	1.12503d-10	4.00	5.25443d-14	6.97

Table 8: Convergence study for Example 3 with seventh order accurate WENO-Z reconstruction and seventh order accurate Runge-Kutta method. The reference solution was computed using method 3 on a grid with 4096×4096 grid cells.

6.2 Test problems with discontinuous solutions

We tested our methods for the standard two-dimensional Riemann problems proposed by Schultz-Rinne [17] and did not observe any numerical problems by using the proposed methods for problems with discontinuities.

In Figures 4 and 5 we show results for [17, configuration 5]. The results obtained by the standard dimension-by-dimension approach and our modified methods compare very well. This is in agreement with observations reported in [25], where it was observed that for problems with discontinuities the classical dimension-by-dimension approach gives as good results as the more expensive formally higher order accurate method. One could easily construct finite volume methods, which only use the modified higher-order accurate update in regions where the solution is smooth (and the modification is justified). Note that we used the WENO-JS instead of the WENO-Z reconstruction (see Appendix B), since this reconstruction produced slightly fewer oscillations behind the discontinuities.

7 A high-order WENO finite volume method for the equations of ideal magnetohydrodynamics

Finally, we apply the modified WENO method to a more complex application, namely the approximation of the 3d ideal magnetohydrodynamic (MHD) equations.

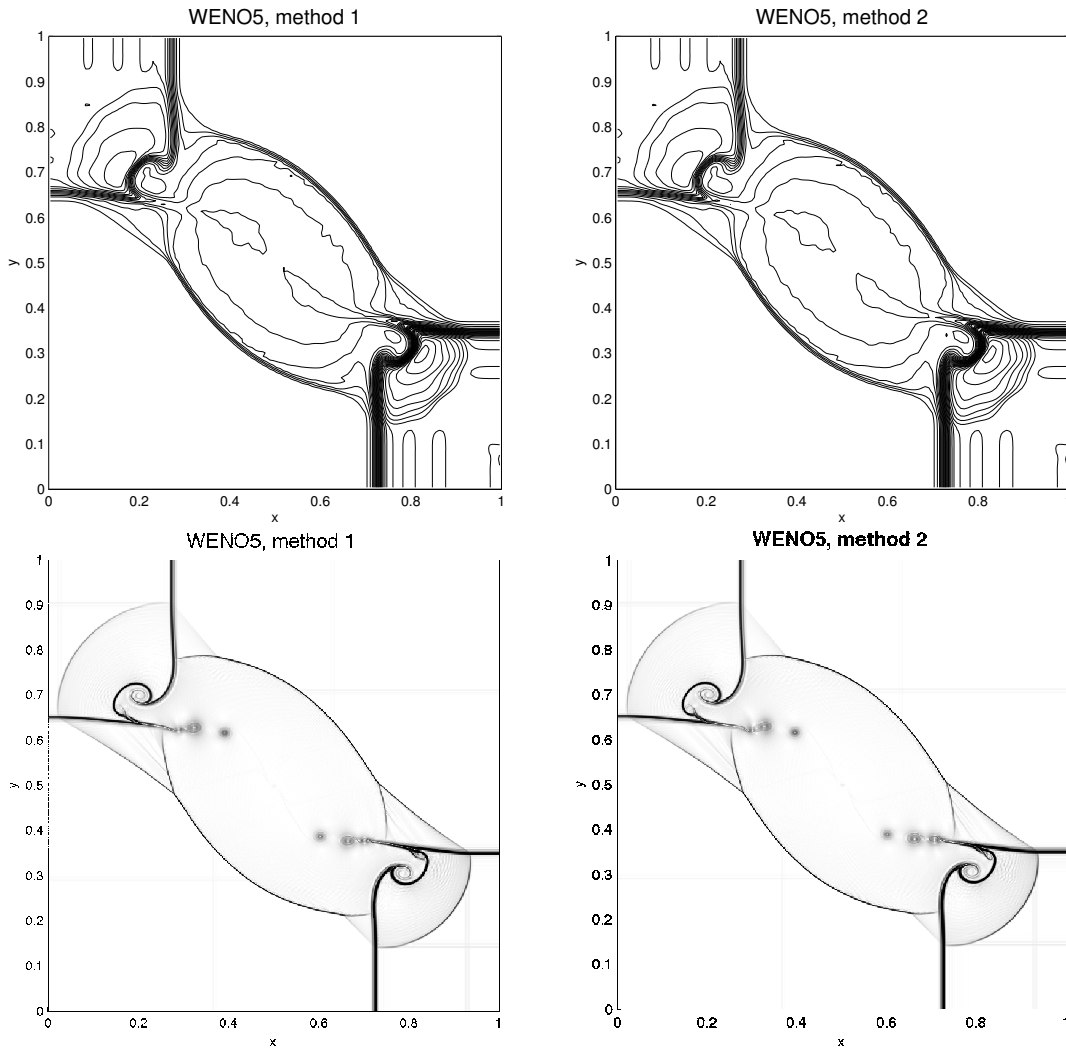


Figure 4: Comparison of method 1 and method 2 for a standard two-dimensional Riemann problem on a grid with (top) 128×128 and (bottom) 1024×1024 grid points. Here we used WENO5 with RK5 and the Roe Riemann solver. We show contour lines of the computed solutions on coarse grids and schlieren plots for the more resolved computations.

The ideal MHD equations can be written in the form

$$\frac{\partial}{\partial t} \begin{pmatrix} \rho \\ \rho \mathbf{u} \\ E \\ \mathbf{B} \end{pmatrix} + \nabla \cdot \begin{pmatrix} \rho \mathbf{u} \mathbf{u} + (p + \frac{1}{2} \|\mathbf{B}\|^2) \mathbb{I} - \mathbf{B} \mathbf{B} \\ \mathbf{u} (E + p + \frac{1}{2} \|\mathbf{B}\|^2) - \mathbf{B} (\mathbf{u} \cdot \mathbf{B}) \\ \mathbf{u} \mathbf{B} - \mathbf{B} \mathbf{u} \end{pmatrix} = 0, \quad (41)$$

$$\nabla \cdot \mathbf{B} = 0,$$

where ρ , $\rho \mathbf{u}$ and E are the total mass, momentum and energy densities, and \mathbf{B} is the magnetic field. The thermal pressure, p , is related to the conserved quantities through the ideal gas law

$$p = (\gamma - 1) \left(E - \frac{1}{2} \|\mathbf{B}\|^2 - \frac{1}{2} \rho \|\mathbf{u}\|^2 \right), \quad (42)$$

where $\gamma = 5/3$ is the ideal gas constant.

It is well known, that numerical methods for the multidimensional MHD equations must control errors in the discrete divergence of the magnetic field. One possibility to do this, is by using so-called constrained transport (CT) methods. Here we use an approach which was recently developed by Helzel, Rossmannith and Taetz [6, 7], and which is based on earlier work by Rossmannith [15]. A

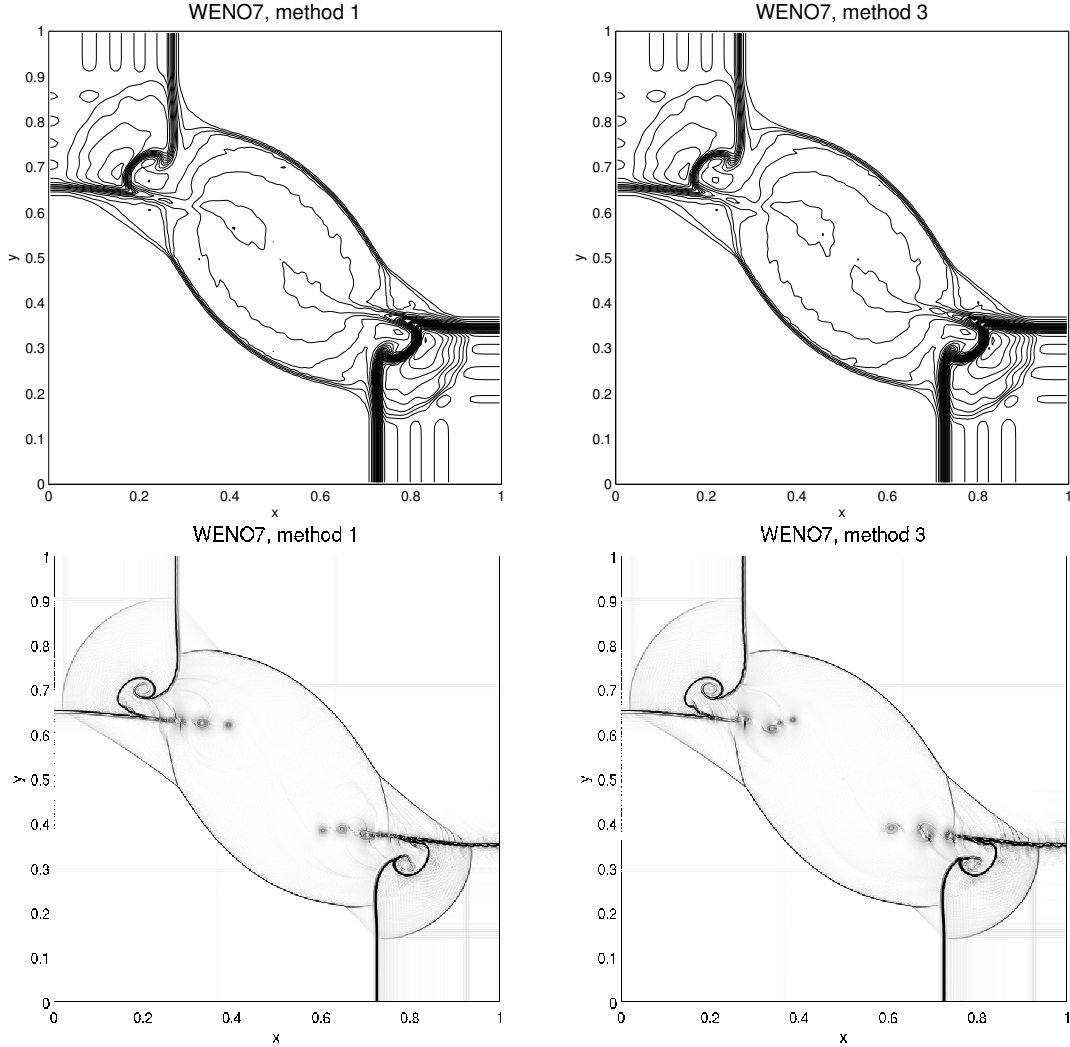


Figure 5: Comparison of method 1 and method 3 for a standard two-dimensional Riemann problem on a grid with (top) 128×128 and (bottom) 1024×1024 grid points. Here we used WENO7 with RK7 and the Roe Riemann solver.

FD-WENO method for the ideal MHD equations, using this same kind of constrained transport, was recently proposed by Christlieb, Rossmannith and Tang [3].

Since \mathbf{B} is divergence free, we can set $\mathbf{B} = \nabla \times \mathbf{A}$, where $\mathbf{A} \in \mathbb{R}^3$ is the magnetic potential. Inserting this relation in the last line of the MHD equations, we derive an evolution equation for the magnetic potential

$$\partial_t \mathbf{A} + (\nabla \times \mathbf{A}) \times \mathbf{u} = -\nabla \phi. \quad (43)$$

Here ϕ is an arbitrary scalar function. Different choices of ϕ represent different *gauge condition* choices as explained in [7]. We use the so-called *Weyl gauge*, which means that we set $\nabla \phi = 0$ in (43). The resulting evolution equation for the magnetic potential can be written in the form

$$\mathbf{A}_t + N_1(\mathbf{u})\mathbf{A}_x + N_2(\mathbf{u})\mathbf{A}_y + N_3(\mathbf{u})\mathbf{A}_z = 0, \quad (44)$$

with

$$N_1 = \begin{pmatrix} 0 & -u^2 & -u^3 \\ 0 & u^1 & 0 \\ 0 & 0 & u^1 \end{pmatrix}, \quad N_2 = \begin{pmatrix} u^2 & 0 & 0 \\ -u^1 & 0 & -u^3 \\ 0 & 0 & u^2 \end{pmatrix}, \quad N_3 = \begin{pmatrix} u^3 & 0 & 0 \\ 0 & u^3 & 0 \\ -u^1 & -u^2 & 0 \end{pmatrix}. \quad (45)$$

The system (44) with matrices of the form (45) is weakly hyperbolic, i.e. the matrix $N(\mathbf{n}) = n^1 N_1(\mathbf{u}) + n^2 N_2(\mathbf{u}) + n^3 N_3(\mathbf{u})$ has real eigenvalues for all $\mathbf{n} \in S^2$, but there are directions for which $N(\mathbf{n})$ fails to have a complete set of right eigenvectors, see [7].

To describe the general form of the constrained transport algorithm, we introduce the notation

$$Q'_{MHD}(t) = \mathcal{L}_1(Q_{MHD}(t)), \quad (46)$$

for the semi-discrete form of the MHD equations. Here $Q_{MHD}(t)$ represents the grid function at time t consisting of all cell-averaged values of the conserved quantities from the MHD equation (41). Analogously, we introduce

$$Q'_{\mathbf{A}}(t) = \mathcal{L}_2(Q_{\mathbf{A}}(t), Q_{MHD}(t)), \quad (47)$$

to describe the semi-discrete form for the evolution equation of the magnetic potential. Note that the evolution of the potential depends on the velocity field, which we take to be as given function from the solution step of the MHD equations.

To simplify notation, we present the numerical method using forward Euler time-stepping.

0. Start with Q_{MHD}^n and $Q_{\mathbf{A}}^n$ (i.e. the solution from the previous time step).
1. Update without regard of the divergence-free condition on the magnetic field, to obtain Q_{MHD}^* and $Q_{\mathbf{A}}^{n+1}$:

$$Q_{MHD}^* = Q_{MHD}^n + \Delta t \mathcal{L}_1(Q_{MHD}^n) \quad (48)$$

$$Q_{\mathbf{A}}^{n+1} = Q_{\mathbf{A}}^n + \Delta t \mathcal{L}_2(Q_{\mathbf{A}}^n, Q_{MHD}^n) \quad (49)$$

2. Correct the magnetic field components Q_{MHD}^* by the divergence-free values $\mathbf{B}^{n+1} = \nabla \times Q_{\mathbf{A}}^{n+1}$. Set $Q_{MHD}^{n+1} = (\rho^{n+1}, \rho \mathbf{u}^{n+1}, E^{n+1}, \mathbf{B}^{n+1})$.

In Step 1, update (48), we use a straight forward extension to the three-dimensional case of our modified WENO method for hyperbolic partial differential equations in divergence form. Here we used the 5th order WENO-Z method with a correction that leads to fourth order accurate flux functions, i.e. method 2.

In Step 1, update (49), we used a three-dimensional extension of our method from Section 4, to update the evolution equation for the magnetic potential. Note that due to the weak hyperbolicity of (44), the fluctuations $\mathbf{A}^{\pm} \Delta Q_{i+\frac{1}{2},j,k}$, $\mathbf{B}^{\pm} \Delta Q_{i,j+\frac{1}{2},k}$ and $\mathbf{C}^{\pm} \Delta Q_{i,j,k+\frac{1}{2}}$ can not be computed using an eigenvector decomposition of the jump in $Q_{\mathbf{A}}$ at grid cell interfaces. Instead, we computed the fluctuations using an approach based on the idea of path conservative methods, as explained in [6].

In Step 2, we compute $\mathbf{B}^{n+1} = (B^1, B^2, B^3)$ from the cell average values of $Q_{\mathbf{A}}^{n+1} = (A^1, A^2, A^3)$, using the formulas

$$\begin{aligned} B_{i,j,k}^1 &= \frac{1}{12\Delta y} (A_{i,j-2,k}^3 - 8A_{i,j-1,k}^3 + 8A_{i,j+1,k}^3 - A_{i,j+2,k}^3) \\ &\quad - \frac{1}{12\Delta z} (A_{i,j,k-2}^2 - 8A_{i,j,k-1}^2 + 8A_{i,j,k+1}^2 - A_{i,j,k+2}^2) \\ B_{i,j,k}^2 &= \frac{1}{12\Delta z} (A_{i,j,k-2}^1 - 8A_{i,j,k-1}^1 + 8A_{i,j,k+1}^1 - A_{i,j,k+2}^1) \\ &\quad - \frac{1}{12\Delta x} (A_{i-2,j,k}^3 - 8A_{i-1,j,k}^3 + 8A_{i+1,j,k}^3 - A_{i+2,j,k}^3) \\ B_{i,j,k}^3 &= \frac{1}{12\Delta x} (A_{i-2,j,k}^2 - 8A_{i-1,j,k}^2 + 8A_{i+1,j,k}^2 - A_{i+2,j,k}^2) \\ &\quad - \frac{1}{12\Delta y} (A_{i,j-2,k}^1 - 8A_{i,j-1,k}^1 + 8A_{i,j+1,k}^1 - A_{i,j+2,k}^1). \end{aligned} \quad (50)$$

This is a fourth order accurate approximation of cell averaged values of $\nabla \times \mathbf{A}$ using cell averaged values of the magnetic potential.

We tested the new finite volume CT method for the 3d smooth Alfvén wave problem. The initial data and the computational domain for this problem are described in [7]. For our computations we used WENO-Z5 + RK5. In Table 9, we show results of a numerical convergence study. There we compare the constrained transport method with our modified WENO method implemented in method 2 with the simple dimension-by-dimension approach implemented in method 1. As expected, we observe second order convergence rates for method 1. Method 2 converges with fourth order.

grid	method 1		method 2	
	$\ \rho - \rho_{ref}\ _1$	EOC	$\ \rho - \rho_{ref}\ _1$	EOC
16x32x32	7.02906d-4		7.81748d-4	
32x64x64	6.23454d-5	3.49	5.28206d-5	3.89
64x128x128	8.02708d-6	2.96	3.36290d-6	3.97
128x256x256	1.57417d-6	2.35	2.11027d-7	3.99
256x512x512	3.68469d-7	2.09	1.31970d-8	4.00

Table 9: Convergence study for smooth Alfvén wave problem using WENO-Z5+RK5 on a three-dimensional Cartesian grid.

Conclusions

We have presented a simple modification of the popular dimension-by-dimension WENO method for Cartesian grids, which retains the full order of accuracy of the corresponding one-dimensional method. Our approach is based on a transformation of interface values and point values of the conserved quantities and numerical flux functions. For the popular WENO5 method, the simplest modification, which we call method 2, gave very good results. For even higher order methods, such as WENO7, we suggest to use the modification according to method 3.

Our method is an alternative to the multi-dimensional WENO finite volume method on Cartesian grids used previously [23, 24, 25]. Compared to theirs, our approach is less expensive. While the computing time for the method in [25] is about 3.3-4.3 times that of the standard dimension-by-dimension approach, our method requires only about 1.1-1.2 times the computing time of the standard method.

For our considerations we always used the simplest version of the finite volume WENO method, where WENO reconstruction is performed component-wise for the conserved quantities. Better results can often be obtained by applying WENO reconstruction to primitive variables or characteristic variables. The modifications suggested in this paper can also be introduced for such methods with only small modifications.

To simplify the notation, we have presented our improved versions of the WENO method for two-dimensional problems. An extension to the three-dimensional case is straight forward and the relevant formulas for a transformation between cell averaged values and point values were presented in Section 5. We have also applied three-dimensional versions of the proposed methods in the framework of unstaggered constrained transport methods for the MHD equations.

Together with Jürgen Dreher, we are currently developing an AMR version of our method.

A Explicit Runge-Kutta methods

For the temporal discretization we use explicit Runge-Kutta methods of order 5 and 7, respectively. After discretizing the PDE in space, we obtain a system of ordinary differential equations of the general form

$$\frac{d}{dt}Q(t) = \mathcal{L}(Q(t)), \quad (51)$$

where $Q(t)$ is a grid function of cell average values of the conserved quantities at time t . We discretize the resulting ode system using Runge-Kutta methods of order five and seven. The methods are described by the Butcher tableaux in Tables 10-11.

0					
$\frac{1}{4}$	$\frac{1}{4}$				
$\frac{1}{4}$	$\frac{1}{8}$	$\frac{1}{8}$			
$\frac{1}{2}$	0	$-\frac{1}{2}$	1		
$\frac{3}{4}$	$\frac{3}{16}$	0	0	$\frac{9}{16}$	
1	$-\frac{3}{7}$	$\frac{2}{7}$	$\frac{12}{7}$	$-\frac{12}{7}$	$\frac{8}{7}$
	$\frac{7}{90}$	0	$\frac{32}{90}$	$\frac{12}{90}$	$\frac{32}{90}$
					$\frac{7}{90}$

Table 10: Butcher tableau of the fifth order accurate Runge-Kutta method from [14].

0													
$\frac{2}{27}$	$\frac{2}{27}$												
$\frac{1}{9}$	$\frac{1}{36}$	$\frac{1}{12}$											
$\frac{1}{6}$	$\frac{1}{24}$	0	$\frac{1}{8}$										
$\frac{5}{12}$	$\frac{5}{12}$	0	$-\frac{25}{16}$	$\frac{25}{16}$									
$\frac{1}{2}$	$\frac{1}{20}$	0	0	$\frac{1}{4}$	$\frac{1}{5}$								
$\frac{5}{6}$	$-\frac{25}{108}$	0	0	$\frac{125}{108}$	$-\frac{65}{27}$	$\frac{125}{54}$							
$\frac{1}{6}$	$\frac{31}{300}$	0	0	0	$\frac{61}{225}$	$-\frac{2}{9}$	$\frac{13}{900}$						
$\frac{2}{3}$	2	0	0	$-\frac{53}{6}$	$\frac{704}{45}$	$-\frac{107}{9}$	$\frac{67}{90}$	3					
$\frac{1}{3}$	$-\frac{91}{108}$	0	0	$\frac{23}{108}$	$-\frac{976}{135}$	$\frac{311}{54}$	$-\frac{19}{60}$	$\frac{17}{6}$	$-\frac{1}{12}$				
1	$\frac{2383}{4100}$	0	0	$-\frac{341}{164}$	$\frac{4496}{1025}$	$-\frac{301}{82}$	$\frac{2133}{4100}$	$\frac{45}{82}$	$\frac{45}{164}$	$\frac{18}{41}$			
	$\frac{41}{840}$	0	0	0	0	$\frac{34}{105}$	$\frac{9}{35}$	$\frac{9}{35}$	$\frac{9}{280}$	$\frac{9}{280}$	$\frac{41}{840}$		

Table 11: Butcher tableau of a seventh order accurate Runge–Kutta method from [5].

In Figure 6 we show the stability regions of the two different Runge–Kutta methods used in this paper.

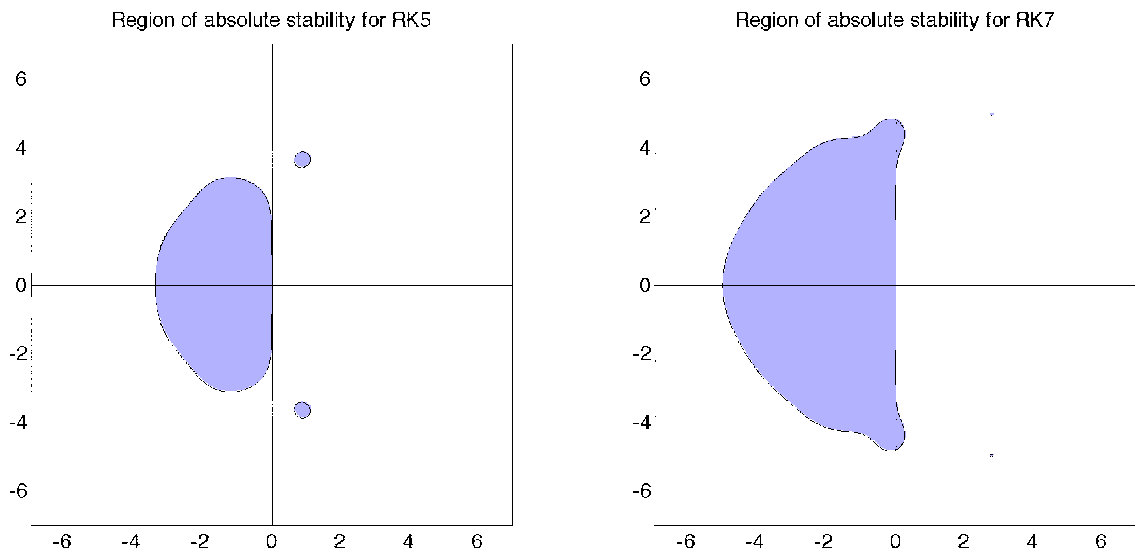


Figure 6: Regions of absolute stability for RK5 and RK7.

B Spatial reconstruction of interface values

In this appendix we give the formulas for the spatial reconstruction of interface averaged values of the conserved quantity used in our implementation of the WENO method. We present the formulas for the reconstruction in the x -direction. This is based on a description of WENO methods in [1, 4, 20].

B.1 5th order accurate WENO reconstruction

At grid cell interfaces we compute averaged values of the conserved quantities

$$Q_{i\pm\frac{1}{2},j}^\mp = w_1^\mp Q_{i\pm\frac{1}{2},j}^{(1\mp)} + w_2^\mp Q_{i\pm\frac{1}{2},j}^{(2\mp)} + w_3^\mp Q_{i\pm\frac{1}{2},j}^{(3\mp)}, \quad (52)$$

with

$$\begin{aligned}
Q_{i+\frac{1}{2},j}^{(1-)} &= \frac{1}{3}Q_{i-2,j} - \frac{7}{6}Q_{i-1,j} + \frac{11}{6}Q_{i,j}, & Q_{i-\frac{1}{2},j}^{(1+)} &= -\frac{1}{6}Q_{i-2,j} + \frac{5}{6}Q_{i-1,j} + \frac{1}{3}Q_{i,j} \\
Q_{i+\frac{1}{2},j}^{(2-)} &= -\frac{1}{6}Q_{i-1,j} + \frac{5}{6}Q_{i,j} + \frac{1}{3}Q_{i+1,j}, & Q_{i-\frac{1}{2},j}^{(2+)} &= \frac{1}{3}Q_{i-1,j} + \frac{5}{6}Q_{i,j} - \frac{1}{6}Q_{i+1,j} \\
Q_{i+\frac{1}{2},j}^{(3-)} &= \frac{1}{3}Q_{i,j} + \frac{5}{6}Q_{i+1,j} - \frac{1}{6}Q_{i+2,j}, & Q_{i-\frac{1}{2},j}^{(3+)} &= \frac{11}{6}Q_{i,j} - \frac{7}{6}Q_{i+1,j} + \frac{1}{3}Q_{i+2,j}.
\end{aligned} \tag{53}$$

The coefficients w_1^\pm, \dots, w_3^\pm in (52) depend on the local solution structure. In the WENO-Z method suggested by Don and Borges [4], they have the form

$$w_j^\pm = \frac{\tilde{w}_j^\pm}{\sum_{i=1}^3 \tilde{w}_i^\pm}, \quad \text{with } \tilde{w}_j^\pm = \gamma_j^\pm \left(1 + \left(\frac{\tau_5}{\beta_j + \epsilon} \right)^p \right), \tag{54}$$

with $p = 2$ and $j = 1, \dots, 3$. $\gamma_1^- = \gamma_3^+ = \frac{1}{10}$, $\gamma_2^- = \gamma_2^+ = \frac{3}{5}$, $\gamma_3^- = \gamma_1^+ = \frac{3}{10}$, β_j as described in [20, Equation (2.9)], $\tau_5 = |\beta_1 - \beta_3|$ and $\epsilon = \Delta x^4$. The WENO-Z methods are constructed to recover the optimal spatial order of convergence. For other high order WENO methods this may depend stronger on the choice of parameters such as ϵ , see for example [8].

The WENO-JS method is obtained by replacing the computation of \tilde{w}_j^\pm by the formula

$$\tilde{w}_j^\pm = \frac{\gamma_j^\pm}{(\epsilon + \beta_j)^2}, \quad j = 1, 2, 3. \tag{55}$$

Here the same values are used for γ_j^\pm and β_j , but the parameter ϵ is replaced by $\epsilon = 10^{-6}$.

B.2 7th order accurate WENO reconstruction

Our seventh order spatial reconstruction uses values $Q^{(1\mp)}, \dots, Q^{(4\mp)}$ from [1] and computes $Q_{i\pm\frac{1}{2},j}^\mp$ analogously to (52), with weights of the same form

$$w_j^\pm = \frac{\tilde{w}_j^\pm}{\sum_{i=1}^4 \tilde{w}_i^\pm}, \quad \text{with } \tilde{w}_j^\pm = \gamma_j^\pm \left(1 + \left(\frac{\tau_7}{\beta_j + \epsilon} \right)^p \right), \tag{56}$$

The β -terms are set to be equal to IS_0^4, \dots, IS_3^4 as defined in [1, page 415]. For the 7th order WENO-Z method we set $\tau_7 = |\beta_1 + 3\beta_2 - 3\beta_3 - \beta_4|$, $p = 2$ and $\epsilon = \Delta x^5$, see [4]. For the 7th order WENO-JS method we use

$$\tilde{w}_j^\pm = \frac{\gamma_j^\pm}{(\epsilon + \beta_j)^2}, \quad j = 1, \dots, 4. \tag{57}$$

with $\epsilon = 10^{-10}$.

References

- [1] D.S. Balsara and C.-W. Shu. Monotonicity preserving weighted essentially non-oscillatory schemes with increasingly high order of accuracy. *J. Comput. Phys.*, 160:405–452, 2000.
- [2] J. Casper and H.L. Atkins. A finite-volume high-order ENO scheme for two-dimensional hyperbolic systems. *J. Comput. Phys.*, 106:62–76, 1993.
- [3] A.J. Christlieb, J.A. Rossmannith and Q. Tang. Finite difference weighted essentially non-oscillatory schemes with constrained transport for ideal magnetohydrodynamics. preprint, 2013.
- [4] W.-S. Don and R. Borges. Accuracy of the weighted essentially non-oscillatory conservative finite difference schemes. *J. Comput. Phys.*, 250: 347–372, 2013.
- [5] E. Fehlberg. Klassische Runge–Kutta-Formeln fünfter und siebenter Ordnung mit Schrittweiten-Kontrolle. *Computing*, 4:93–106, 1969.

- [6] C. Helzel, J.A. Rossmannith, and B. Taetz. A high order unstaggered constrained transport method for the ideal magnetohydrodynamic equations based on the method of lines. *SIAM J. Sci. Comput.*, 35:A623–A651, 2013.
- [7] C. Helzel, J.A. Rossmannith, and B. Taetz. An unstaggered constrained transport method for the 3d ideal magnetohydrodynamic equations. *J. Comput. Phys.*, 230: 3803–3829, 2011.
- [8] A.K. Henrick, T.D. Aslam, and J.M. Powers. Mapped weighted essentially non-oscillatory schemes: Achieving optimal order near critical points. *J. Comput. Phys.*, 207:542–567, 2005.
- [9] C. Hu and C.-W. Shu. Weighted essentially non-oscillatory schemes on triangular meshes. *J. Comput. Phys.*, 150:97–127, 1999.
- [10] D.I. Ketcheson, M. Parsani, and R.J. LeVeque. High-order wave propagation algorithms for hyperbolic systems. *SIAM J. Sci. Comput.*, 35:A351–A377, 2013.
- [11] R.J. LeVeque. *Finite Volume Methods for Hyperbolic Problems*. Cambridge University Press, 2002.
- [12] P. McCorquodale and P. Colella. A high-order finite volume method for conservation laws on logically refined grids. *Commun. App. Math. and Comp. Sci.*, 6:1–25, 2011.
- [13] B. Merriman. Understanding the Shu–Osher conservative finite difference form. *J. Sci. Comput.*, 19:309–322, 2003.
- [14] F. Rabiei and F. Ismail. Fifth-order improved Runge-Kutta methods with reduced number of function evaluations. *Australian Journal of Basic and Applied Sciences*, 6:97–105, 2012.
- [15] J.A. Rossmannith. An unstaggered, high-resolution constrained transport method for magnetohydrodynamic flows. *SIAM J. Sci. Comput.*, 28:1766–1797, 2006
- [16] P. Tsoutsanis, V.A. Titarev, and D. Drikakis. Weno schemes on arbitrary mixed-element unstructured meshes in three space dimension. *J. Comput. Phys.*, 230:1585–1601, 2011.
- [17] C.W. Schultz-Rinne. Classification of the Riemann problem for two dimensional gas dynamics. *SIAM J. Math. Anal.*, 24:76–88, 1993.
- [18] C. Shen, J.M. Qiu and A. Christlieb. Adaptive mesh refinement based on high order finite difference WENO scheme for multi-scale simulations. *J. Comput. Phys.*, 230:3780–3802, 2011.
- [19] Y. Shen and G. Zha. Improved seventh-order WENO schemes. *AIAA Paper*, 2010-1451.
- [20] C.-W. Shu. High order weighted essentially nonoscillatory schemes for convection dominated problems. *SIAM Review*, 51:82–126, 2009.
- [21] C.-W. Shu and S. Osher. Efficient implementation of essentially non-oscillatory shock-capturing schemes. *J. Comput. Phys.*, 77:439–471, 1988.
- [22] C.-W. Shu and S. Osher. Efficient implementation of essentially non-oscillatory shock-capturing schemes, II. *J. Comput. Phys.*, 83:32–78, 1989.
- [23] J. Shi, C. Hu and C.-W. Shu. A technique for treating negative weights in WENO schemes. *J. Comput. Phys.*, 175:108–127, 2002.
- [24] V.A. Titarev and E.F. Toro. Finite-volume WENO schemes for three-dimensional conservation laws. *J. Comput. Phys.*, 201:238–260, 2004.
- [25] R. Zhang, M. Zhang, and C.-W. Shu. On the order of accuracy and numerical performance of two classes of finite volume WENO schemes. *Commun. Comput. Phys.*, 9:807–827, 2011.